3
Motor-cart-pendulum system: introduction of a mechanical energy reservoir

The second electromechanical system analyzed in this Thesis has the same elements of the first system and a pendulum that is embarked into the cart, as shown in Fig. 3.1. Its suspension point is fixed in the cart, hence moves with it. The main point here is that the pendulum can have a relative motion with respect to the cart.

3.1 Dynamics of the motor-cart-pendulum system

The pendulum is modeled as a mathematical pendulum (bar without mass and particle of mass m_p at the end). Its length is noted as l_p and the pendulum angular displacement as θ. The equations of the cart-pendulum were obtained with the Lagrange principle. They are

$$m_p l_p^2 \ddot{\theta}(t) + m_p l_p \ddot{x}(t) \cos\theta(t) + m_p g_a l_p \sin\theta(t) = 0 \ , \tag{3.1}$$

$$(m_p + m_c)\ddot{x}(t) + m_p l_p \ddot{\theta}(t) \cos\theta(t) - m_p l_p \dot{\theta}^2(t) \sin\theta(t) = f(t) \ , \tag{3.2}$$

where, again, f represents the horizontal coupling force between the DC motor and the cart, g_a is the acceleration of gravity, and the horizontal cart displacement is x. The mass of the mechanical system, m, is equal the cart mass plus the pendulum mass, $m_c + m_p$. The relative motion of the embarked pendulum causes a variation in the position of the center of mass of the mechanical system. As in the first coupled system, the cart is not allowed to move in the vertical direction. Due to the problem geometry, $x(t)$ and $\alpha(t)$

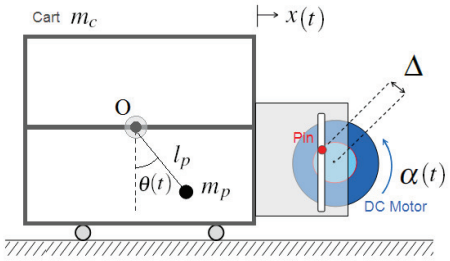

Figure 3.1: Cart-motor-pendulum system.

are related by Eq. (2.9). Once again, it is assumed that the motor shaft is rigid and that there is no friction between the pin and the slot. Thus, the available torque to the coupled mechanical system, $\boldsymbol{\tau}$, is written as Eq. (2.6). Substituting the Eq. (2.7), (2.9), (3.1) and (3.2) into Eqs. (2.1) and (2.2), we obtain the initial value problem for the motor-cart-pendulum system that is written as follows. Given a constant source voltage ν, find (α, c, θ) such that, for all $t > 0$,

$$
\begin{aligned}
& l\dot{c}(t) \quad + rc(t) + k_e\dot{\alpha}(t) = v \ , \\
& \\
& \ddot{\alpha}(t) \quad \left[j_m + (m_c + m_p)\Delta^2(\sin\alpha(t))^2\right] + k_e\, c(t) \\
& \qquad + \dot{\alpha}(t)\ \left[b_m + (m_c + m_p)\Delta^2\dot{\alpha}(t)\cos\alpha(t)\ \sin\alpha(t)\right] \\
& \qquad - \ddot{\theta}(t)\ \left[m_p l_p \cos\theta(t)\Delta\sin\alpha(t)\right] + \dot{\theta}(t)\ \left[m_p\, l_p\dot{\theta}(t)\sin\theta(t)\Delta\sin\alpha(t)\right] = 0 \ , \\
& \\
& \ddot{\theta}(t) \quad \left[m_p\, l_p^2\right] - \ddot{\alpha}(t)\ \left[m_p\, l_p\ \cos\theta(t)\Delta\sin\alpha(t)\right] \\
& \qquad - \dot{\alpha}(t)\ \left[m_p\, l_p\cos\theta(t)\Delta\cos\alpha(t)\dot{\alpha}(t)\right] + \ m_p\, g_a\, l_p\sin\theta(t)\ =\ 0 \ ,
\end{aligned}
\tag{3.3}
$$

with the initial conditions,

$$
\dot{\alpha}(0) = 0 \quad , \quad \alpha(0) = 0 \quad , \quad \dot{\theta}(0) = 0 \quad , \quad \theta(0) = 0 \quad , \quad c(0) = \frac{\nu}{r} . \tag{3.4}
$$

Observing Eq. (3.3), it is verified that the motor-pendulum system influences the cart in a parametric way.

3.2 Dimensionless cart-motor-pendulum system

In this section, the initial value problem to the motor-cart-pendulum system is presented in a dimensionless form. Taking $\dot{\alpha}(t) = u(t)$ and $\dot{\theta}(t) = n(t)$, the system can be written as a first order system

$$\dot{c}(t) = \frac{-k_e u(t) - rc(t) + \nu}{l},$$

$$\begin{aligned}\dot{u}(t) = \; & \{-n(t)^2 m_p l_p \sin\theta(t)\Delta\sin(\alpha(t)) - u(t)^2(m_c+m_p)\Delta^2\cos(\alpha(t))\sin(\alpha(t)) \\ & -b_m u(t) + k_e c(t) + [\cos(\theta(t))\Delta\sin(\alpha(t))]\,[u(t)^2 m_p\cos\theta(t)\Delta\cos\alpha(t) \\ & -m_p g_a\sin(\theta(t))\,]\,\} \\ & \left\{\frac{1}{j_m + \Delta^2\sin(\alpha(t))^2(m_c + m_p\sin(\theta(t))^2)}\right\},\end{aligned}$$

$$\begin{aligned}\dot{n}(t) = \; & \{m_p\cos(\theta(t))\Delta\sin(\alpha(t))\,[k_e c(t) - u(t)^2(m_c+m_p)\Delta^2\cos(\alpha(t))\sin(\alpha(t)) \\ & -b_m u(t) - n(t)^2 m_p l_p\sin\theta(t)\Delta\sin(\alpha(t))\,] + \left[j_m + (m_p+m_c)\Delta^2\sin(\alpha(t))^2\right] \\ & [-m_p g_a\sin(\theta(t)) + u(t)^2 m_p\cos\theta(t)\Delta\cos\alpha(t)]\,\} \\ & \left\{\frac{1}{m_p l_p\left[j_m + \Delta^2\sin(\alpha(t))^2(m_c + m_p\sin(\theta(t))^2)\right]}\right\}.\end{aligned} \tag{3.5}$$

Writing

$$\begin{aligned} & t = \frac{l}{r}s, \quad \alpha\left(\frac{l}{r}s\right) = \gamma(s), \quad u\left(\frac{l}{r}s\right) = \frac{rq(s)}{l}, \quad \theta\left(\frac{l}{r}s\right) = \beta(s), \\ & n\left(\frac{l}{r}s\right) = \frac{ry(s)}{l}, \quad c\left(\frac{l}{r}s\right) = \frac{k_e w(s)}{l},\end{aligned} \tag{3.6}$$

one gets that s is dimensionless parameter. The functions $\gamma(s)$, $q(s)$, $\beta(s)$, $y(s)$ and $w(s)$ are dimensionless functions. By substituting Eq. (3.6) into Eq. (3.5) one obtains

$$w'(s) = -w(s) - q(s) + v_0\,,$$

$$\begin{aligned}q'(s) = \; & \{-v_3 q(s) - y(s)^2 v_5\sin(\gamma(s))\sin(\beta(s)) - v_6\sin(\beta(s))\cos(\beta(s))\sin(\gamma(s)) \\ & +v_2 w(s) - q(s)^2\cos(\gamma(s))\sin(\gamma(s))\left[v_9 - v_4\cos(\beta(s))^2\right] \\ & \left\{\frac{1}{1+\sin(\gamma(s))^2\left[v_1 + v_4\sin(\beta(s))^2\right]}\right\}\end{aligned} \tag{3.7}$$

$$\begin{aligned}y'(s) = \; & \{-v_3 v_7 q(s)\cos(\beta(s))\sin(\gamma(s)) + q(s)^2 v_7\cos(\gamma(s))\cos(\beta(s)) \\ & -v_4 y(s)^2\sin(\gamma(s))^2\sin(\beta(s))\cos(\beta(s)) + v_2 v_7 w(s)\cos(\beta(s))\sin(\gamma(s)) \\ & \left[1 - v_9\sin(\gamma(s))^2\right][-v_8\sin(\beta(s))]\,\}\left\{\frac{1}{1+\sin(\gamma(s))^2\left[v_1 + v_4\sin(\beta(s))^2\right]}\right\},\end{aligned} \tag{3.8}$$

where $'$ denotes the derivative with respect to s and a_i, $i = 1, \cdots, 16$ are dimensionless parameters given by

$$v_0 = \frac{\nu l}{k_e r}, \quad v_1 = \frac{\Delta^2 m_c}{j_m}, \quad v_2 = \frac{l k_e^2}{j_m r^2}, \quad v_3 = \frac{b_m l}{j_m r}, \quad v_4 = \frac{\Delta^2 m_p}{j_m},$$
$$v_5 = \frac{m_p l_p \Delta}{j_m}, \quad v_6 = \frac{m_p \Delta g_a l^2}{j_m r^2}, \quad v_7 = \frac{\Delta}{l_p}, \quad v_8 = \frac{g_a l^2}{l_p r^2}, \quad v_9 = \frac{(m_c + m_p)\Delta^2}{j_m}. \tag{3.9}$$

Comparing the dimensionless parameters of the motor-cart-pendulum system with the dimensionless parameters of the motor-cart system given by Eq. 2.16, it can be observed that the parameters v_0 to v_3 appear in both cases and, the inclusion of the embarked pendulum introduces six news parameters: v_4 to v_9.

3.3 Numerical simulations of the dynamics of the motor-cart-pendulum system

A similar analysis to the one made to the motor-cart system, based on the results of numerical simulations, was developed for the motor-cart-pendulum system. The 4th-order Runge-Kutta method is used for the time-integration scheme with a time-step equal to 10^{-4}. The motor parameters used in all simulations are listed in Table 2.1. The source voltage is assumed to be constant in time and equal to 2.4 V. Despite of using the dimensionless initial value problem for numerical simulations, the results are presented in the dimensional form because we believe that in this way they have an easier physical interpretation. Looking at the initial value problem Eqs. (3.3) to (3.4), it is observed that if the nominal eccentricity of the pin, Δ, is small and the angle, $\theta(t)$, is near zero, Eq. (3.3) tends to a linear system. But as the eccentricity grows, the nonlinearities become more pronounced. To understand the influence of Δ in the dynamic behavior of the motor-cart system, simulations with two different values to this system parameter were performed. The selected values are $\Delta = 0.001$ m and $\Delta = 0.01$ m. In these simulations, the cart and the pendulum masses were $m_c = 0.0$ kg and $m_p = 5.0$ kg, so that the total mass, $m = m_c + m_p = 5.0$ kg, is equal to the embarked mass. Although the masses are equal, this configuration contrasts with the one of the motor-cart system used in the previous simulations. In spite of having the same masses, the pendulum has a relative motion with respect to the cart, and this makes a huge difference. The pendulum length was assumed to be 0.075 m. For $\Delta = 0.001$ m, Figs. 3.2(a), 3.2(b), 3.3(a) and 3.3(b) show the graphs of the angular velocity of the motor shaft, current, pendulum displacement and cart displacement over time. These results reveal that when Δ is small, the angular speed of the motor shaft oscillates over time with a very small amplitude around 7 Hz, the current also oscillates with a small amplitude around 0.13 A, and the angular displacement of pendulum is near

zero. The Fast Fourier Transform was computed to the cart and pendulum

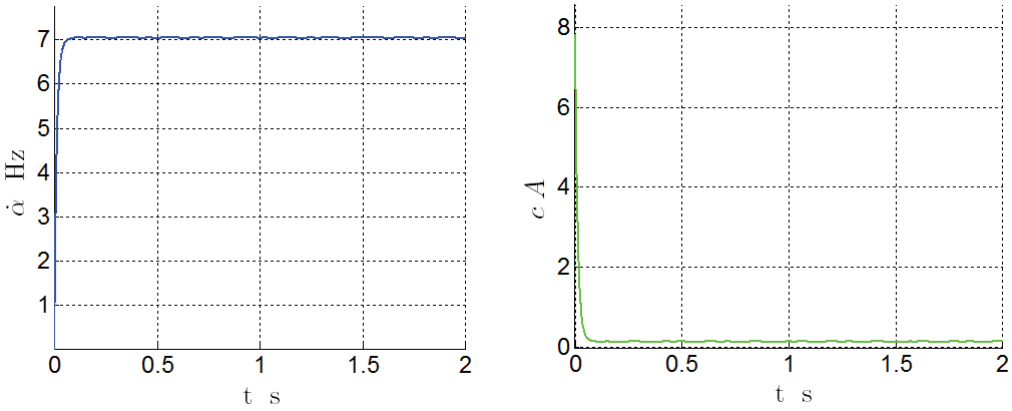

3.2(a): 3.2(b):

Figure 3.2: Motor-cart-pendulum system with $\Delta = 0.001$ m: (a) angular velocity of the motor shaft and (b) current over time.

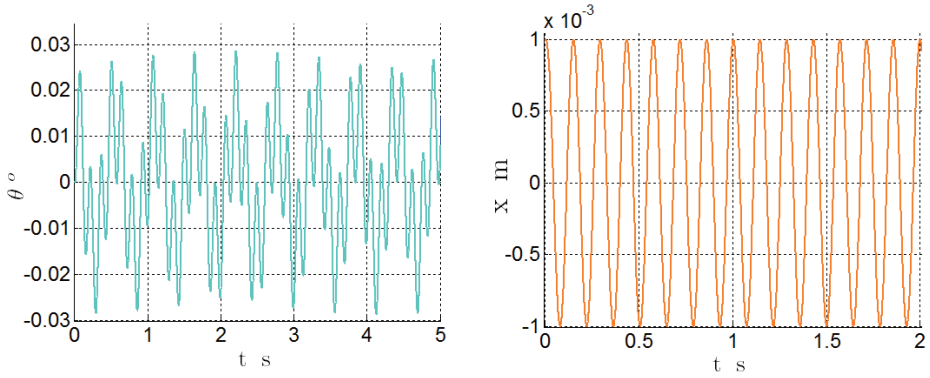

3.3(a): 3.3(b):

Figure 3.3: Motor-cart-pendulum system with $\Delta = 0.001$ m: (a) pendulum displacement and (b) cart displacement over time.

displacements and to the current for this small value of Δ. The obtained graphs are shown in Figs. 3.4(a) and 3.4(b). The FFT graph of $\hat{x}$, shown in Fig. 3.4(a), presents only one peak at the frequency at 7.04 Hz. This peak was expected, since this is close to the angular speed of the motor shaft. The FFT graph of $\hat{\theta}$ presents two peaks. One of them coincides with the $\hat{x}$ peak and the other one is at the natural frequency of the pendulum, i.e., $\omega_n = \sqrt{g/l_p}/(2\pi) = 1.82$ Hz. The FFT graph of $\hat{c}$ presents three peaks. The first one is at 5.22 Hz, the second on is at 8.86 Hz and the third one at 14.08 Hz, that is twice the peak frequency of the FFT $\hat{x}$. This relation 2:1 between the peak frequency of $\hat{c}$ and $\hat{x}$ indicates the parametric excitation. Figures 3.5(a), 3.5(b), 3.6(a) and 3.6(b) show the graphs of angular speed of the motor, current, pendulum and

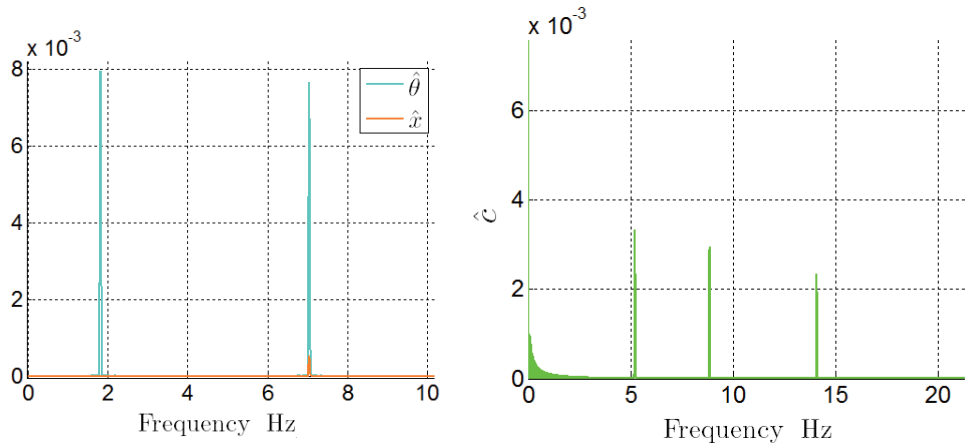

3.4(a): 3.4(b):

Figure 3.4: Motor-cart-pendulum system with $\Delta = 0.001$ m: Fast Fourier Transform of (a) cart and pendulum displacements and (b) of current.

cart displacement over time when $\Delta = 0.01$ m. Comparing these graphs with Figs. 3.2(a), 3.2(b), 3.3(a) and 3.3(b), It is verified that with a bigger Δ, the amplitude of the oscillations of $\dot{\alpha}$, c, and θ in the steady state will be also bigger. As done to the results with small Δ, the FFT was computed to the

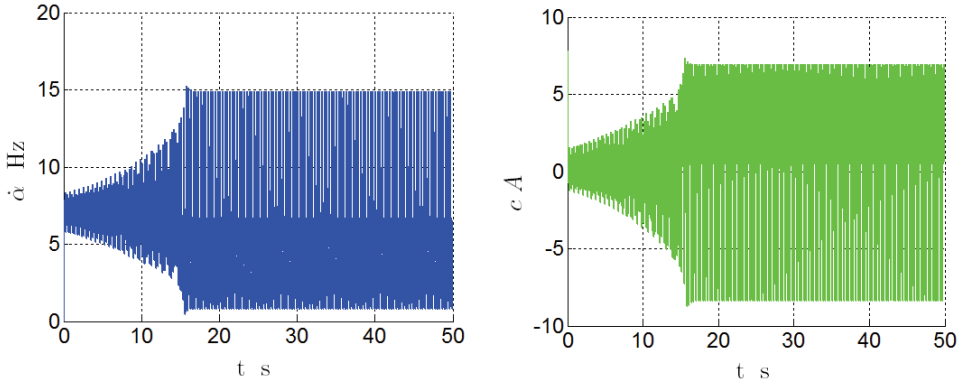

3.5(a): 3.5(b):

Figure 3.5: Motor-cart-pendulum system with $\Delta = 0.01$ m: (a) angular velocity of the motor shaft and (b) current over time.

cart and pendulum displacements, angular speed of the motor shaft and to the current for the new value of Δ. Figures 3.7(a), 3.7(b), 3.7(a), 3.7(b) display the obtained graphs. Observing Figs. 3.7(a) and 3.7(b), it can be noted that $\hat{x}$ and $\hat{\theta}$ present peaks at the same frequencies. The first of them is at 1.61 Hz and the following are at odd multiples of this value. Comparing $\hat{x}$ with $\Delta = 0.001$ m and with $\Delta = 0.01$ m, it is verified that the peak at the natural frequency of the pendulum, $\omega_n = 1.82$ Hz, vanished when Δ grows. This result certifies that the system behavior is far from linear. Regarding Figs. 3.8(a) and 3.8(b),

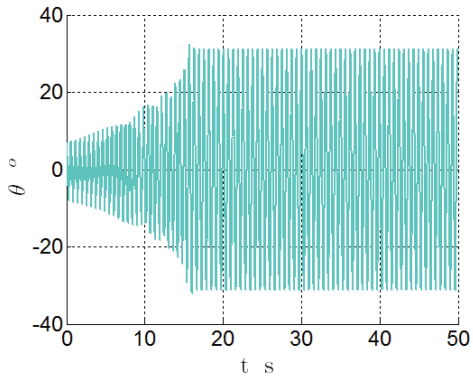

3.6(a):

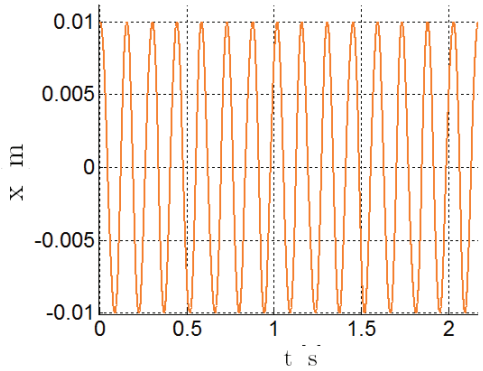

3.6(b):

Figure 3.6: Motor-cart-pendulum system with $\Delta = 0.01$ m: (a) pendulum and (b) cart displacement over time.

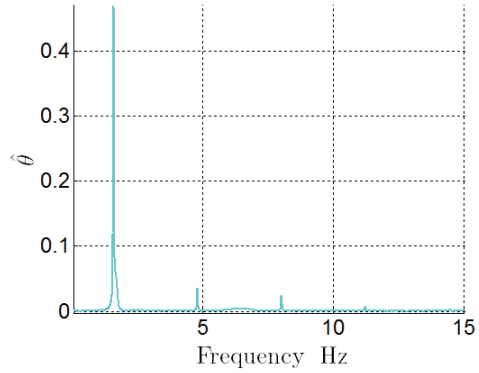

3.7(a):

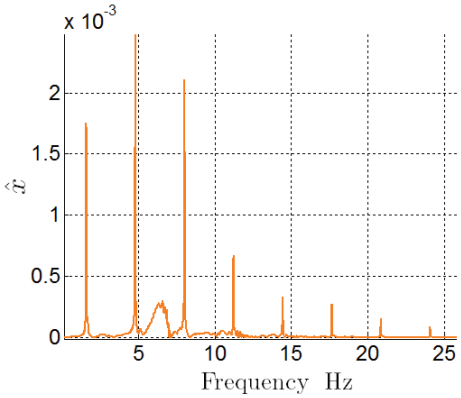

3.7(b):

Figure 3.7: Motor-cart-pendulum system with $\Delta = 0.01$ m: Fast Fourier Transform of (a) pendulum and (b) cart displacements.

it can be noted that the FFT graphs of the current and of the angular speed of the motor shaft over time also present peaks at the same frequencies. The first of them is at 3.21 Hz and the following are at multiples of this value. Comparing Figs. 3.8(a) and 3.7(b), it can be verified that the frequencies in which $\hat{c}$ presents peaks are twice the frequencies in which $\hat{x}$ presents peaks.

3.4 Pumping Leads To Revolution

In Section 3.3, the cart mass was considered to be zero and the pendulum mass 5.0 kg. Next, it is presented an analysis of the behavior of this system with a different mass configuration. The cart mass is kept as 0.0 kg (a limit case) and a smaller value is selected to the pendulum mass, $m_p = 4.0$ kg, so that the total mass, $m_c + m_p = 4.0$ kg, is still equal to the embarked mass. Figures 3.9(a), 3.9(b), 3.10(a) and 3.10(b) show the graphs of the angular speed

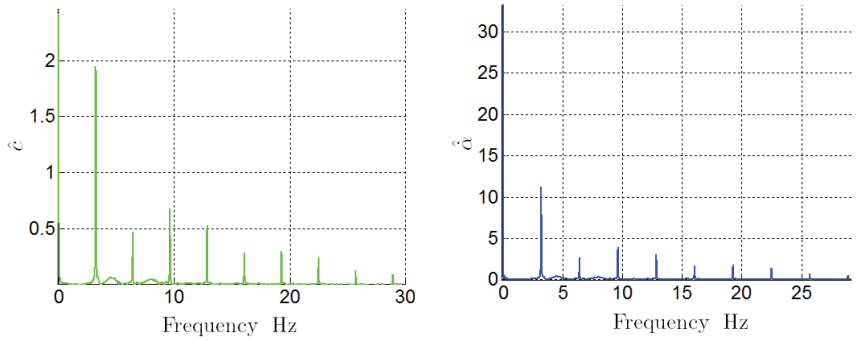

3.8(a): 3.8(b):

Figure 3.8: Motor-cart-pendulum system with $\Delta = 0.01$ m: Fast Fourier Transform of (a) current and (b) angular speed of the motor shaft over time.

of the motor shaft, current and cart and pendulum displacements over time for this new mass configuration when $\Delta = 0.01$ m. Regarding these graphs, it can be observed that after the transient state, the dynamics achieves a periodic state, in which $\dot{\alpha}$ takes negatives values. With this new mass configuration, the mechanical system pumps energy from the motor and the amplitude of the pendulum grows reaching a point where the mechanical system starts to drive the motion, [30, 29, 12]. This is seen observing that $\dot{\alpha}$ takes negative values, indicating that the motor shaft sometimes changes its motion direction. When the angular speed of the motor shaft is positive, it is considered that the motor drives the cart motion, the cart is driven. But when it is negative, the motor looses the control over the cart and drives it no more, it is now driven by the mechanical system. In these situations, it will be said that the relation master-slave is reversed. To understand the sign changing of the angular speed

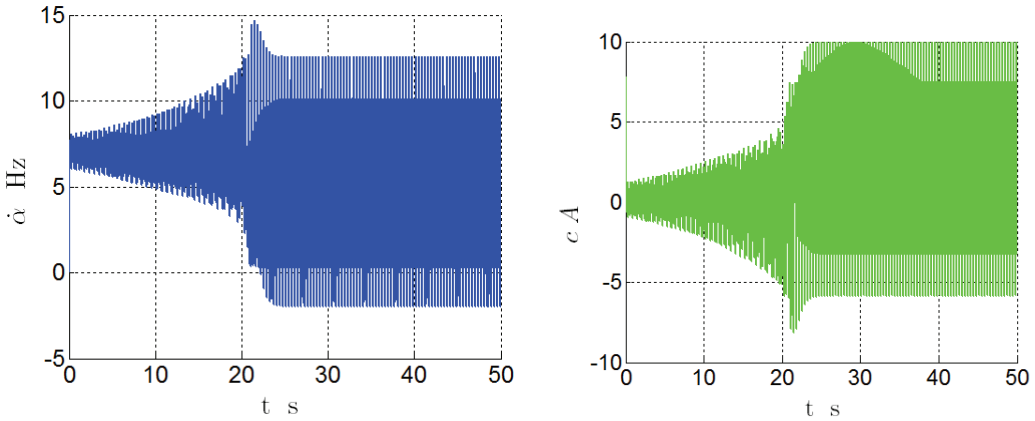

3.9(a): 3.9(b):

Figure 3.9: Motor-cart-pendulum system with $\Delta = 0.01$ m: (a) angular velocity of the motor shaft and (b) current over time.

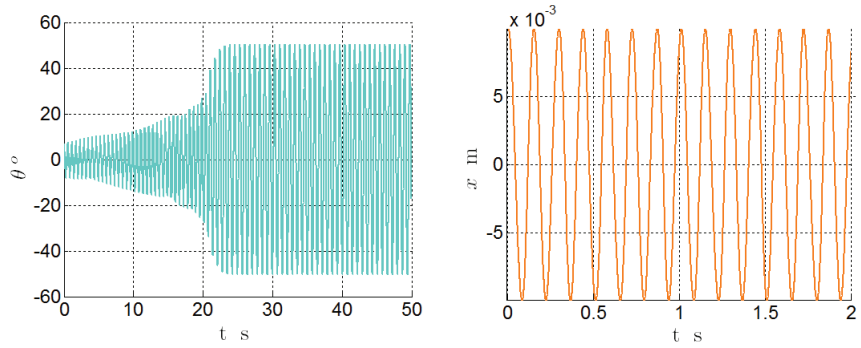

3.10(a): 3.10(b):

Figure 3.10: Motor-cart-pendulum system with $\Delta = 0.01$ m: (a) pendulum and (b) cart displacement over time.

of the motor shaft, some phase portrait graphs were plotted. Figures 3.11(a) and 3.11(b) show the $\ddot{\alpha}$ graph as function of $\dot{\alpha}$ and the $\dot{\alpha}$ graph as function of x during one movement cycle. It is verified that when $\dot{\alpha}(t)$ turns negative, the motor shaft has a negative acceleration. After a short period of time, its acceleration becomes positive and brakes the motor shaft motion. This causes other sign changing in $\dot{\alpha}(t)$ and consequently, it turns positive again. Thus, the motor recovers the control over the cart motion. Looking at Fig. 3.11(b),

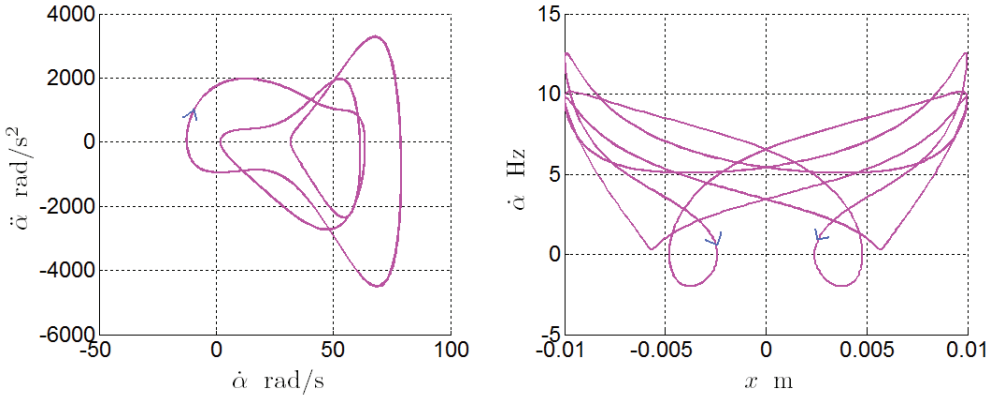

3.11(a): 3.11(b):

Figure 3.11: Motor-cart-pendulum system with $\Delta = 0.01$ m: portrait graphs of (a) $\ddot{\alpha}$ graph as function of $\dot{\alpha}$ and (b) $\dot{\alpha}$ graph as function of x.

it is noted that this reversion in the relation master-slave occurs two times in each movement cycle. The position and angular speed of the pendulum, at the moment of the reversion, can be observed by the graphs of $\dot{\theta}$ as function of $\dot{\alpha}$ and θ in function of $\dot{\alpha}$, shown in Figs. 3.12(a) and 3.12(b). It is verified that when the the motor looses the control over the cart by the sign changing of $\dot{\alpha}$, the pendulum angle is around 21.6^o or around -21.6^o. When the motor recovers the control, the pendulum angle is around 6.0^o or around -6.0^o. It

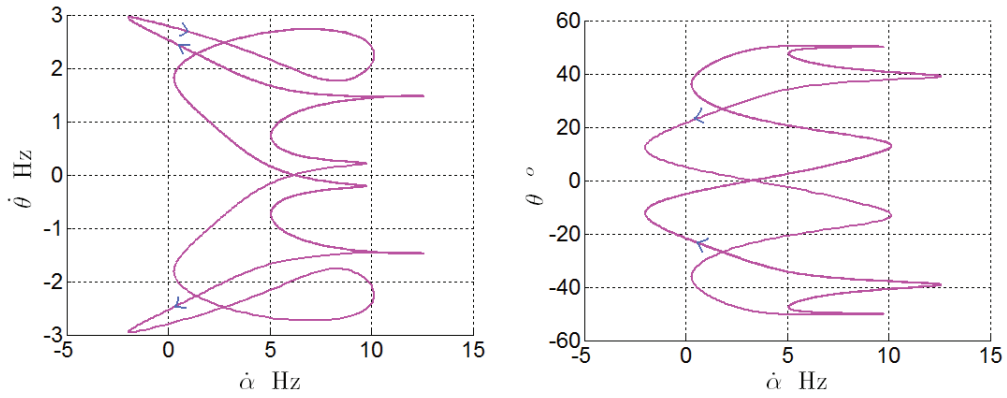

3.12(a): 3.12(b):

Figure 3.12: Motor-cart-pendulum system with $\Delta = 0.01$ m: portrait graphs of (a) $\dot{\theta}$ graph as function of $\dot{\alpha}$ and (b) θ as function of $\dot{\alpha}$.

is also noted that, during the period of reversion, the pendulum does not change its direction of motion in spite of its angular speed presents a change of behavior. In the beginning of the reversion the modulus of $\dot{\theta}$ grows, but when it achieves the value 2.95 Hz, it starts to decrease. This change occurs due to the sign changing in the tangent angular acceleration of the pendulum, as can be observed in Fig. 3.13(a). The graph of the torque variation in function of the angular speed of the motor shaft shows that the maximum torque is achieved during the period of reversion.

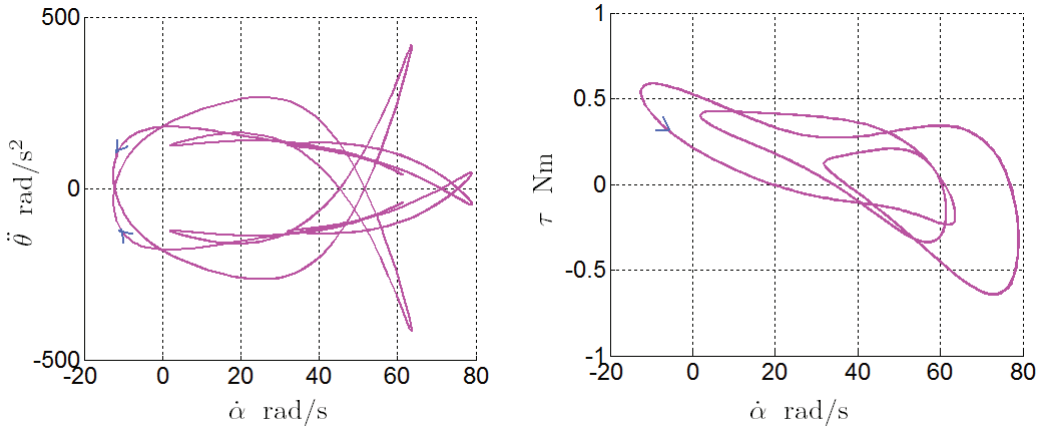

3.13(a): 3.13(b):

Figure 3.13: Motor-cart-pendulum system with $\Delta = 0.01$ m: portrait graphs of (a) tangent $\ddot{\theta}$ graph as function of $\dot{\alpha}$ and (b) τ as function of $\dot{\alpha}$.

3.5 Summary of the Chapter

The influence of a embarked mass was demonstrated and it was shown the changes it causes in the solutions of the dynamic equations. The motor-cart system has no capacity to pump energy from the motor, it is a master-slave system: the motor drives the cart motion, the cart is driven. The only interesting feature is how the nonlinearity changes with Δ and m, the mass of the cart. The motor-cart-pendulum system has a new feature, the capacity to store energy in the motion of the pendulum. With this, the mechanical system can pump energy from the motor and, in certain cases, revert the relation master-slave, that is the mechanical system can be itself the master stopping the motor and reversing its motion.